Influence of size on the compressive properties of cellular structures manufactured by additive technologies

Wpływ rozmiaru na właściwości ściskające struktur komórkowych wytwarzanych technologiami przyrostowymi

MATEUSZ RUDNIK *

This article is a continuation of research on hexagonal cell structures. Previous research has dealt with cell structures in normalized models, where it was shown that cell structures should be studied from a single cell to a suitably generated iterative model based on recursive formulas. The aim of this paper was to compare manufactured cell structures with an appropriately defined formula. Printed models of the hexagonal structure subjected to compression showed that, in the case of the Polylactic Acid Blue material, as the size of the side length of the hexagonal cells increased, the quality of the generated diagrams also increased, which informed the undesired effects of the compressive force in the tests. In the case of cells manufactured from the PA2200 material, it was noted that the maximum force acting on the cell structure decreased with increasing cell side length, however, no undesirable situations occurred during testing in contrast to structures manufactured from Polylactic Acid base materials. In the case of Polylactic Acid materials, special attention had to be paid to the Polylactic Acid Gray material. The models were printed with the same parameters, from the same Stereolitography language file, had a slightly higher mass and were subjected to the same compression test, yet showed significant differences in the tests carried out compared to the other models.
KEYWORDS: PLA, PA2200, FFF, SLS, cell structures, additive manufacturing

Artykuł jest kontynuacją badań dotyczących struktur komórkowych heksagonalnych. Poprzednie badania dotyczyły struktur komórkowych w modelach znormalizowanych. Wykazano, że struktury komórkowe należy badać od pojedynczej komórki do odpowiednio wygenerowanego modelu iteracyjnego opartego na wzorach rekurencyjnych. Celem pracy było porównanie wytworzonych struktur komórkowych o odpowiednio zdefiniowanym wzorze. Wydrukowane modele struktury heksagonalnej poddanej ściskaniu wykazały, że w przypadku materiału Polylactic Acid Blue wraz ze wzrostem długości boku komórek heksagonalnych wzrastała także jakość generowanych diagramów, co informowało o niepożądanych efektach działania siły ściskającej. W przypadku struktur komórkowych wykonanych z materiału PA2200 zauważono, że maksymalna siła działająca na strukturę komórkową zmniejszała się wraz ze wzrostem długości boku struktury komórkowej, jednakże podczas badań nie wystąpiły żadne niepożądane sytuacje w porównaniu ze strukturami wytwarzanymi z materiałów na bazie kwasu polimlekowego. W przypadku materiałów z polikwasu mlekowego szczególną uwagę należało zwrócić na materiał z szarego kwasu polimlekowego. Modele zostały wydrukowane z tymi samymi parametrami, z tego samego pliku, który został zapisany w języku stereolitograficznym, a jednak miały nieco większą masę i zostały poddane temu samemu testowi ściskania, a mimo to wykazały istotne różnice w przeprowadzonych testach w porównaniu z pozostałymi modelami.
SŁOWA KLUCZOWE: PLA, PA2200, FFF, SLS, struktury komórkowe, wytwarzanie przyrostowe

Introduction

Belonging to Industry 4.0, additive technologies offer the possibility to set values for a large variety of technological parameters of 3D printing, which have an impact on the properties of the manufactured finished product. In some articles researchers used polylactic acid or a combination with other polymers is the most commonly used material in fused deposition modeling technology (FDM/FFF) [1–3].

The infill patterns used make it possible to minimize the material usage. However, this affects the mechanical properties of the models manufactured. Different approaches to the problem of cellular structures are emerging in research concepts around the world. One concept was to design cubes with a significant number of cells in the structure. The models were further used to test mechanical, thermal and chemical properties. Another of the concepts used was to inscribe the cellular structure in standardized models. This type of study of cellular structures provided an opportunity to refer to material studies in standardized models. The method offered the possibility of obtaining a model with similar mechanical properties.

Another type of study of cellular structures was the design of structures from a single cell. Cellular bonding manufactured models with different mechanical properties. This provided the opportunity to make parts with cellular structures in technologies where the infill pattern option was not possible. However, this involved time-consuming development of an optimalised cell structure for a specific model [4–6].

* Mgr inż. Mateusz Rudnik – mrudnik@tu.kielce.pl, 0000-0001-5096-608X – Department of Mechanical Engineering and Engineering Technology, Kielce University of Technology, Kielce, Poland

Increasingly, mixed structures can be used in so-called sandwich structures in composite models [7]. However, in the case of cell structures, the problem of thin-walledness arises, which is an ongoing issue in 2D and 3D printing of cell structures [8, 9].

Combining the concept of modelling cellular structures from single cell with the ability to use an appropriate infill pattern with Fused Filament Fabrication technology allowed models with more complex cellular structures to be manufactured. This provided an opportunity to study the mechanical properties of cellular structures identified as being similar in structure to fractals. The resemblance to fractals, made it possible to apply the resulting cellular structures to different models according to suitably selected patterns [10]. However, applying them to a specific model took away one of the features linking the manufactured detail with the cellular structure and the fractals. Despite the similarity itself, the model was finite and had a permanent structure defined by the material used and the printed part. The tests performed can be used to determine which force would need to be used for relaxation and creep tests of models with cell structures.

One of the types of studies of cell structures was relaxation studies, where a number of samples were made, which were then intended for such a study [11]. The relaxation phenomenon is a broadly built issue, where the parameterization of mathematical models in 3D printing is very complicated [12, 13].

In the publication Zhang et al. [14] a study of the bending properties of samples with biomimetic sandwich cell structures inspired by elytrons were presented. The samples were manufactured from nylon by selective laser sintering technology. Bending was performed by using a three-point method. The results exhibited that the performance of TBEP (a type of biomimetic sandwich structure inspired by the beetle elytron) in three-point bending could also be improved by setting appropriate TBEP panel radii and chamfers; excessive increases in these radii could result in a reduced mechanical performance [14].

In the following article, four orders of hierarchical structures based on the Menger cube were investigated and subjected to mechanical, electrical and thermal tests, where a range of variability was demonstrated after a decrease in density, and it was shown that a Menger sponge with a hexagonal cavity would have the lowest normalized thermal and electrical conductivity as the effective density decreased and an increase in the order of the fractal leads to a near-zero Poisson's ratio [15]. A large number of articles base their research on the generation of beams, which are then subjected to bending tests that make it possible to determine a wide range of coefficients and variables relevant to the selection of the appropriate material or infill pattern [16, 17]. From a fractal point of view, however, the infinite possibility of generating cells should be constantly emphasized [18, 19]. However, the only limitation to making a sufficient number of iterations is the type of 3D printer used to print each component.

Samples preparation

The samples generated for testing were created by using a hexagonal cell model. The first step was to generate additional cells with the constraints that two cells be generated on four opposite sides so that the base of this simple cell structure could be aligned parallel to the plane during the compression test. The second step was to cut a space offset by 1 mm of a regular hexagon, which was characterized by the formula:

$$\forall_{n \in N} \, \exists_{I_n, C_n} \left(\begin{cases} I_0 = B_1 - B_2 \\ C_1 = 1 \\ C_n = C_1 + 2n - 2 \\ I_n = I_0 + \cdots + [(4n - C_n)B_1 - 4nB_2] \\ V = I_n H \end{cases} \right)$$

The formula presented features the following designations:
- n – number of iterations,
- I_0 – field of the first hexagonal cell,
- B_1, B_2 – the field of the outer solid of the hexagonal cell and the area of the cut-out,
- C_1, C_n – the first and n-th word of the sequence, respectively defined as the repetition of the sides of the generated regular hexagons, where, as a result of divisibility by 6 (the number of sides of the hexagon), the value of the n-th expression of the sequence was written as the number of hexagons,
- I_n – field of all generated hexagonal cells with cut-outs,
- V, H – volume and height of a solid.

In the research, we only focus on the first iteration, where four additional cells of the same side length were generated. In the study, the cell structure constructed from hexagonal structures with sides $a_1 = 5$ mm, $a_2 = 6$ mm, $a_3 = 7$ mm and height $H = 10$ mm. The cells were assembled in the middle of the side walls to create a wall thickness of $t = 1$ mm. The dimension A based on the formula for the height of an equilateral triangle, on the basis of which the hexagonal structure was presented. This dimension was four times the height of a triangle with side a_n. The B dimension consisted of the two diagonals of the hexagonal structure and the remaining common part of the central cell of the structure. The data presented in table I illustrate the preparation of the experiment, where 60 samples printed from four types of material, in two technologies with three side lengths, were established.
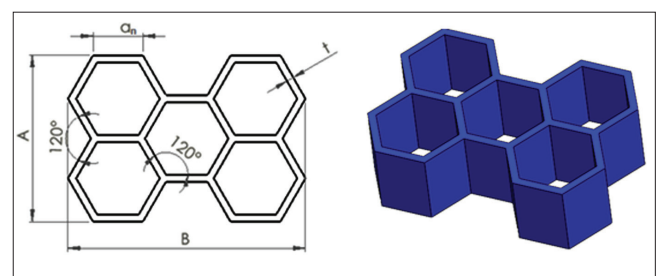
Fig. 1. Hexagonal structure

TABLE I. Design of experiment

	Type of material												
	PA2200			PLAG			PLAW			PLAB			
Length of side [mm]	5	6	7	5	6	7	5	6	7	5	6	7	Total
Sample quantity	5	5	5	5	5	5	5	5	5	5	5	5	60

Materials and Methods

Materials

The material used to model the cell structures from FFF/FDM technology was PLA (Polylactic Acid), the characteristics of which are shown in table II. The material is characterized by biodegradability only for certain dyes and low processing shrinkage in the range of 0.3÷0.5%. The ability to print at nozzle temperatures in the range of 175÷235°C, as well as table temperatures of 0÷60°C [20].

The material used to model the cell structures from SLS technology was PA2200 (Polyamid 2200), the characteristics of which were shown in table III. The material is a white powder based on polyamide 12 (PA12). According to EN ISO 10993-1 and USP/level VI/121°C, the material is considered biocompatible and has been approved for food contact in accordance with EU Directive 2002/72/EC (excluding alcohol products) [21].

TABLE II. Technical data sheet PLA

Mechanical properties	Test method	Typical value
Tensile strength at yield [MPa]	ISO 527	49.5
Tensile strength at break [MPa]	ISO 527	45.6
Tensile modulus [MPa]	ISO 527	2346.5
Elongation at yield [%]	ISO 527	3.3%
Elongation at break [%]	ISO 527	5.2%
Flexural modulus [MPa]	ISO 178	103
Flexural strength [MPa]	ISO 178	3150
PLA B	Color of material	Blue
PLA W		White
PLA G		Gray
Density [g/cc]	–	1.25

TABLE III. Technical Data Sheet PA2200

Mechanical properties	Test method	Typical value
Tensile modulus [MPa]	ISO 527-1/-2	1700
Tensile strength [MPa]	ISO 527-1/-2	50
Elongation at break [%]	ISO 527-1/-2	20
Flexural modulus [MPa]	ISO 178	1500
Izod impact strength [kJ/m^2]	ISO 180/1A	4.4
Thermal properties [Unit]	Test method	Typical value
Melting temperature [°C]	ISO 11357-1/-3	176
Vicat softening temperature [°C]	ISO 306	163
Density [g/cc]	EOS-Method	0.90÷0.95

Methods

The samples were manufactured by fused deposition modeling (FDM) technology on the Makerbot Sketch. The printer is characterized by a table that moves in the Y axis and a print head that moves in the X and Z axes. The aforementioned 3D printing technology uses plastic materials in the form of a filament, which is then deposited at a set temperature on a working platform, where the head from which the filament is extracted increases the ceiling by a set layer thickness. The printer prints from PLA, PLA Tough and PLA materials with minimal admixtures of other materials. The printer has a heated build platform with a temperature range of 0÷100°C. The models were printed according to the same print parameters [22]:
- extruder temperature: 215°C,
- build plate temperature: 60°C,
- layer thickness: 0.2 mm,
- infill pattern: linear,
- infill density: 95%,
- travel speed: 80 mm/s.

The models were printed according to the same print parameters:
- energy density: 0.056,
- layer thickness: 0.1 mm,
- laser type: CO_2 [23].

The compression test was performed on an Inspect Mini 3 kN machine. Applying the fixed test parameters shown in table III. For the compression test, HP23 rigid discs of $A = \varnothing 56$ mm diameter in aluminum material, nickel plating and $B = \varnothing 15.9$ mm mounting were used. The constant parameters for the compression test included a strain of 3 mm and a test speed of 0.5 mm/min. The compression test was achieved with the LabMaster software.

Discussion

The main goal of the work is to demonstrate the relationship between the increase in the side size of the hexagonal structure in the first iteration and the indicated mass and maximum force applied to the model for four materials. At the work is innovative in terms of the dependence of the cellular structure model on the recursive formula generated as part of the expansion of scientific research activities as part of mathematics studies combined with a doctorate in the discipline of mechanical engineering. Cell merging involves disabling the duplication of hexagonal models on the same wall when a uniform model shape is used. With reference to table IV, it can be seen that the weight of the models printed from the PLAG material is slightly higher than the models made from the other two materials. This fact can be

TABLE IV. Characteristics of hexagonal samples

Type of material	PA2200			PLAB		
Type of sample	Mass [g]	Density [g/cc]	Max. load [N]	Mass [g]	Density [g/cc]	Max. load [N]
5Hex1	0.93	0.91	226.52	0.92	0.90	82.40
5Hex2	0.92	0.90	222.46	0.93	0.91	87.79
5Hex3	0.93	0.91	228.48	0.93	0.91	87.59
5Hex4	0.94	0.92	227.59	0.94	0.92	55.55
5Hex5	0.93	0.91	219.72	0.93	0.91	90.42
$\bar{X}$	0.93	0.912	224.954	0.93	0.912	80.750
σ	0.007	0.007	3.722	0.007	0.007	14.384
6Hex1	1.12	0.88	143.78	1.23	0.97	71.41
6Hex2	1.11	0.88	159.44	1.23	0.97	78.39
6Hex3	1.11	0.88	157.41	1.22	0.96	72.20
6Hex4	1.11	0.88	152.00	1.21	0.96	74.51
6Hex5	1.13	0.89	148.61	1.23	0.97	75.59
$\bar{X}$	1.116	0.881	152.248	1.224	0.966	74.420
σ	0.009	0.007	6.391	0.009	0.007	2.79
7Hex1	1.31	0.87	105.39	1.44	0.96	60.42
7Hex2	1.30	0.86	113.12	1.42	0.94	70.18
7Hex3	1.31	0.87	108.26	1.41	0.94	75.13
7Hex4	1.33	0.88	101.42	1.41	0.94	68.28
7Hex5	1.27	0.84	97.52	1.41	0.94	69.23
$\bar{X}$	1.304	0.865	105.142	1.418	0.941	68.648
σ	0.022	0.015	6.029	0.013	0.009	5.304
Type of material	PLAG			PLAW		
Type of sample	Mass [g]	Density [g/cc]	Max. load [N]	Mass [g]	Density [g/cc]	Max. load [N]
5Hex1	1.01	0.99	103.65	0.97	0.95	128.43
5Hex2	1.02	1.00	72.82	0.96	0.94	84.09
5Hex3	1.02	1.00	94.02	0.95	0.93	100.72
5Hex4	1.02	1.00	101.85	0.94	0.92	124.40
5Hex5	1.03	1.01	80.06	0.93	0.91	117.99
$\bar{X}$	1.02	1	90.480	0.95	0.931	111.126
σ	0.007	0.007	13.562	0.016	0.016	18.452
6Hex1	1.29	1.02	68.52	1.21	0.96	71.59
6Hex2	1.28	1.01	71.48	1.21	0.96	67.9
6Hex3	1.29	1.02	73.83	1.20	0.95	65.2
6Hex4	1.28	1.01	72.47	1.21	0.96	61.37
6Hex5	1.29	1.02	64.34	1.21	0.96	64.58
$\bar{X}$	1.286	2.015	70.128	1.208	0.954	66.128
σ	0.005	0.004	3.778	0.004	0.004	3.836
7Hex1	1.54	1.02	57.63	1.45	0.96	57.87
7Hex2	1.55	1.03	62.43	1.44	0.96	57.01
7Hex3	1.54	1.02	57.99	1.43	0.95	55.41
7Hex4	1.54	1.02	61.11	1.44	0.96	56.48
7Hex5	1.53	1.02	58.67	1.44	0.96	59.67
$\bar{X}$	1.540	1.022	59.566	1.440	0.956	57.288
σ	0.007	0.005	2.099	0.007	0.005	1.602

observed for each model of the hexagonal structure, even though they were manufactured from the same stereolithographic file and with constant printing parameters.

For the PA2200 material, the density values oscillate around 90 g/cc and as the side size increases, its mass increases while the density decreases. In the case of models manufactured of PLAB material, the density of the models first increases and then decreases as the side increases. In the case of the hexagonal structure made of PLAG material, the models showed a much higher density compared to other models, and the density values range around $1.01 \div 1.02$ g/cc.

A similar situation occurs for models printed from PLAW material, where the increase in mass does not affect the decrease/increase in density. According to the manufacturer, the density of the PLA material is 1.25 g/cc, the density of PA2200 is, according to the EOS method, between 0.9 and 0.95 g/cc. Models manufactured from the PLAB material exhibited the lowest force decrease. The maximum force set for models with hexagonal structures made from this material oscillated between $60 \div 90$ N, even though the mass of the models was slightly less than that of models made from the other materials.

In the case of the PLAW material, it was noted that the highest values of maximum force for the length of the side $a_1 = 5$ mm. However, the maximum force values for the a_2 and a_3 sides were in the $55 \div 72$ N range.

A similar situation was observed with the PLAG material, where, despite the slightly higher mass of each of the cellular structure models, a higher standard deviation for maximum force was recorded for the a_1-sided structure, however, the force adopted values for in the range $72 \div 104$ N. According to the determined characterics, it can be concluded that for PLAB material the values are clustered closest in the case of side a_1 and a_2. In the case of side a_3, the values are most closely clustered for models manufactured from PLAW material.

The maximum force value for the samples manufactured from PA2200 material was 228.48 N. For all samples manufactured from PA2200 material, the maximum forces were higher than those from PLA materials, but for the 6 and 7 mm side models the standard deviation was twice as high as for the 5 mm side samples.

In contrast to PLA samples, the samples manufactured from PA2200 showed a higher compressive strength, the results were more concentrated around a single value and the load-displacement plots showed that the samples had a similar behaviour in spite of the increase in side length, as shown in the plots in figure 2. The maximum strength for models manufactured by SLS technology is almost twice as high as for FFF technology. The difference in figures 2 a–c results from the fact that despite the same print parameters, STL model, generation using the same mathematical
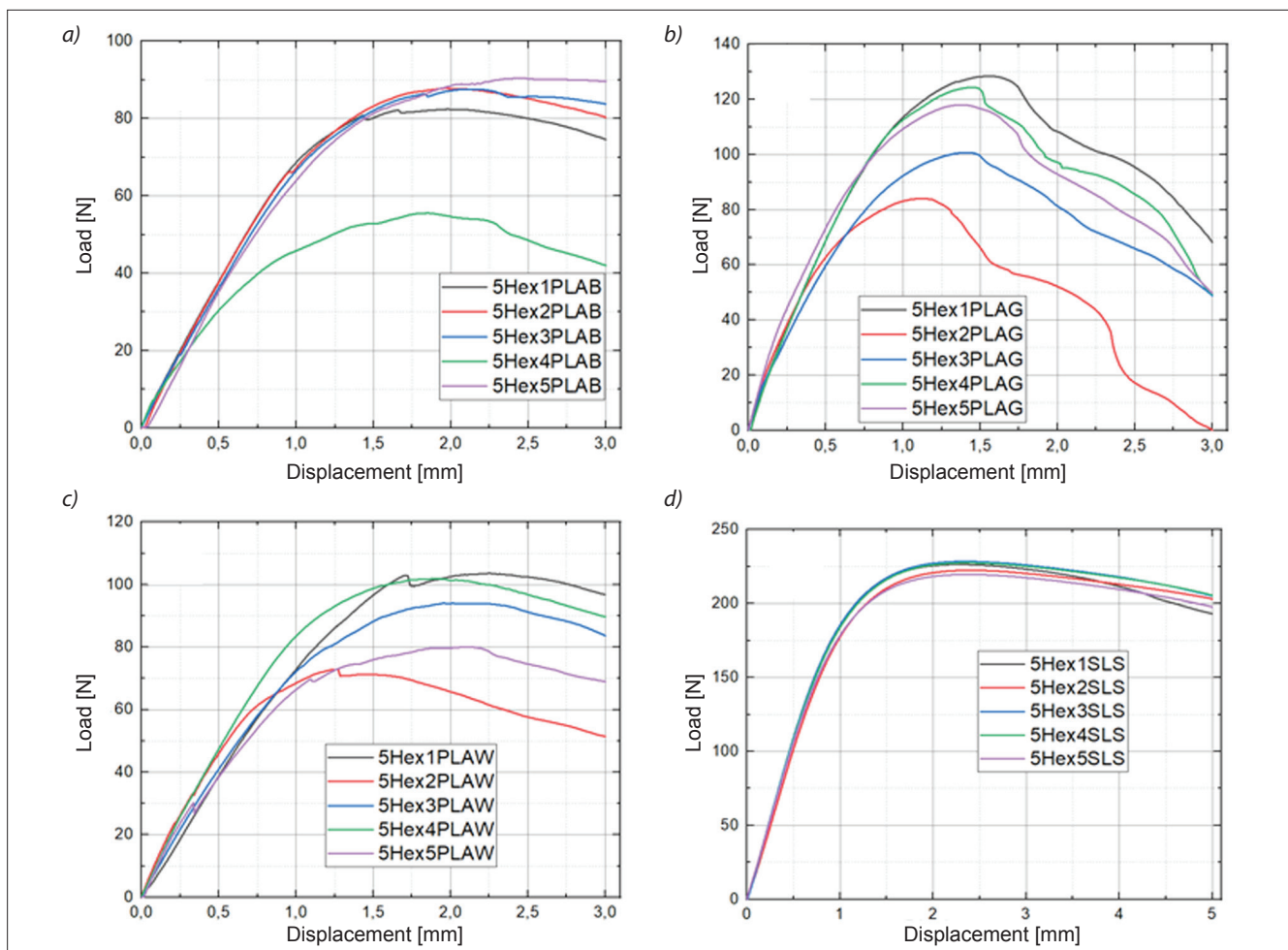
Fig. 2. Plots Load – Displacement – Side $a_1 = 5$ mm: *a)* FDM-PLAB; *b)* FDM-PLAG; *c)* FDM-PLAW; *d)* SLS-PA2200
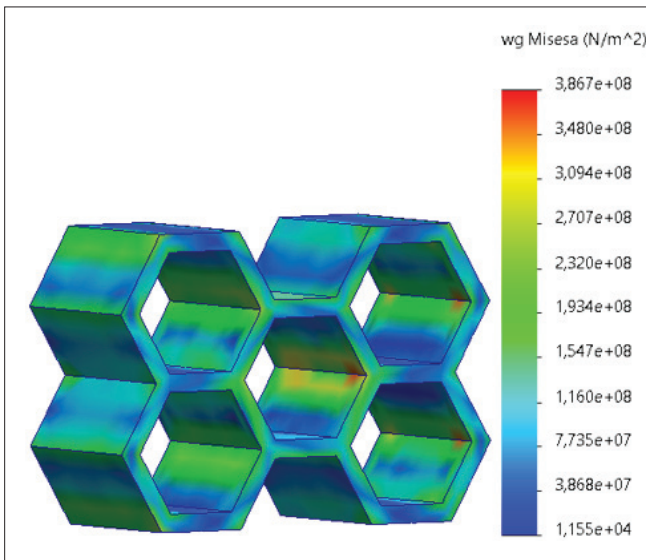
Fig. 3. Collapsing model of cell structure

crepancies, which we will not notice in models made using SLS technology. The second thing concerns the size of the cells, i.e. 5 mm.

The samples are much smaller than the others and, in this case, they cause duality of the graph, where two sectors of cells work. In the first case, the upper and middle cells are destroyed by compression, and in the second stage, as a result of the inclination of the hexagon walls at an angle of 60°, a blockage of the model is generated and the phenomenon of collapse occurs, which was to be captured in the presented graphs. It should be noted that despite the difference in the forces set for the samples, only samples made of PLAG material show a significant decrease in force, almost to 0, which concerned the phenomenon of complete collapse of the cellular structure i.e. Figure 3. Red circles mark the places of breakdown of the cellular structure. Black arrows indicate the direction in which the walls move during the compression test.

Models manufactured from PLA materials showed similar maximum force values. However, each sample from this range of materials had a different behavior when a compressive force was applied. In the case of the PLAB material samples, there was a partial collapse of the upper part of the model which is characterized in Figure 4 by the *a* diagram between 2÷2.5 mm. In the case of the PLAG material samples, it was noted that the models collapsed after reaching the

model, similar mass and density of the set load values, it was noticed, among others, the phenomenon of skipping paths on the Makerbot Sketch printer, where, despite generating a model with a fill level of 95%, there are two types of risks for thin-walled cellular structures. The first concerns the relationship of the cells, which, as one model, should cause uniform stress distribution, however, the height of the layer and the holes between the models cause these dis-

Fig. 4. Plot Load – Displacement – Side a_3 = 6 mm: *a)* FFF-PLAB; *b)* FFF-PLAG; *c)* FFF-PLAW; *d)* SLS-PA2200
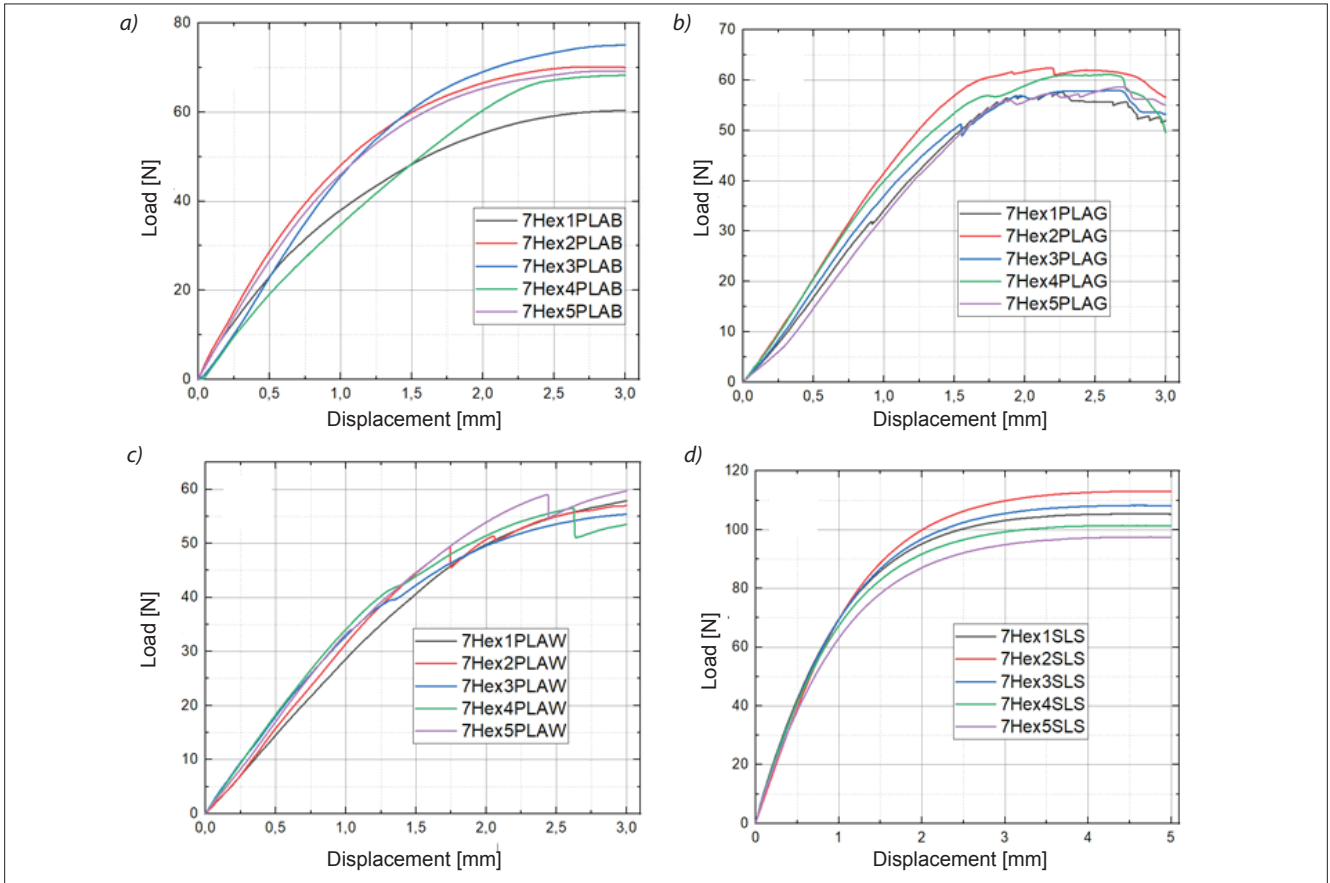
Fig. 5. Plot Load – Displacement – Side $a_3 = 7$ mm: *a*) FDM-PLAB; *b*) FDM-PLAG; *c*) FDM-PLAW; *d*) SLS-PA2200
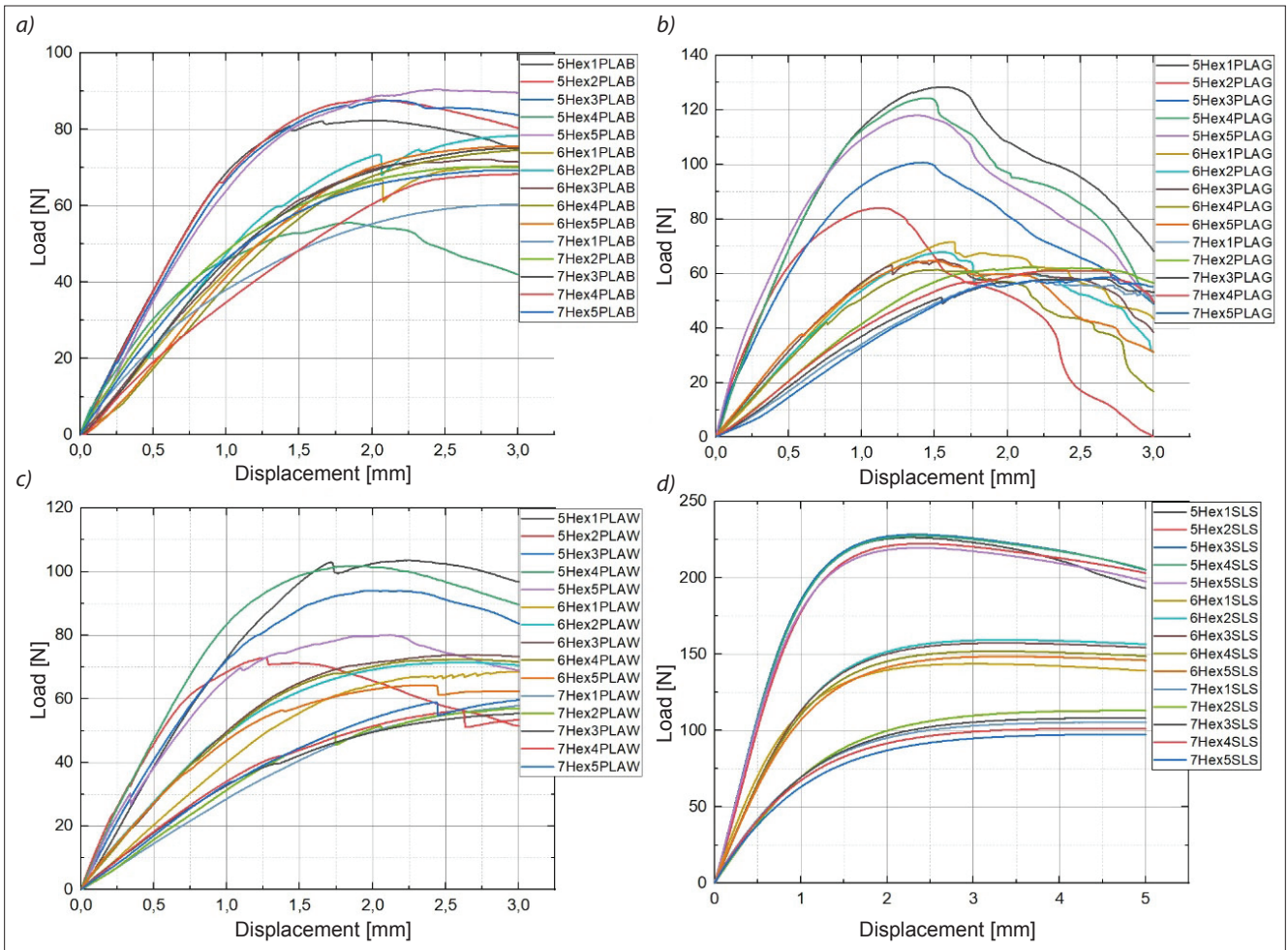
Fig. 6. Summary Plots Load – Displacement: *a*) FDM-PLAB; *b*) FDM-PLAG; *c*) FDM-PLAW; *d*) SLS-PA2200

TABLE V. Correlation between Side-Mass, Side-Load, Mass-Load

Material type	PA2200					
Characteristics	Side [mm]	Mass [g]	Load [N]	Side-Mass	Side-Load	Mass-Load
Average value	6	1.17	160.78	6.82	924.75	172.08
Standard deviation, σ	0.845	0.159	51.268	0.134	43.329	8.131
Expected value, E	X	X	X	6.70	964.69	179.54
cov(x,y)	X	X	X	0.12	−39.94	−7.46
$r(x,y)$	X	X	X	0.9301	−0.9217	−0.9178
Population	15	df	13	$p = 0.05$	0.5139	Statistically significant
Material type	PLAB					
Characteristics	Side [mm]	Mass [g]	Load [N]	Side-Mass	Side-Load	Mass-Load
Average value	6	1.19	74.61	7.31	443.60	87.81
Standard deviation, σ	0.845	0.159	51.268	0.134	43.329	8.131
Expected value, E	X	X	X	7.14	447.63	88.83
cov(x,y)	X	X	X	0.16	−4.03	−1.02
$r(x,y)$	X	X	X	0.9259	−0.4883	−0.5017
Population	15	df	13	$p = 0.05$	0.5139	Statistically significant Side-Mass
Material Type	PLAG					
Characteristics	Side [mm]	Mass [g]	Load [N]	Side-Mass	Side-Load	Mass-Load
Average value	6	1.28	73.39	7.87	430.04	91.39
Standard deviation, σ	0.845	0.208	0.775	0.176	8.261	2.032
Expected value, E	X	X	X	7.69	440.35	94.09
cov(x,y)	X	X	X	0.17	−10.30	−2.70
$r(x,y)$	X	X	X	0.9329	−0.7966	−0.8029
Population	15	df	13	$p = 0.05$	0.5139	Statistically significant
Material type	PLAW					
Characteristics	Side [mm]	Mass [g]	Load [N]	Side-Mass	Side-Load	Mass-Load
Average value	6	1.20	78.18	7.36	451.14	89.30
Standard deviation, σ	0.845	0.207	26.413	0.175	22.323	5.478
Expected value, E	X	X	X	7.20	469.08	93.76
cov(x,y)	X	X	X	0.16	−17.95	−4.46
$r(x,y)$	X	X	X	0.9319	−0.8039	−0.8142
Population	15	df	13	$p = 0.05$	0.5139	Statistically significant

maximum force in the range of 1.5÷2 mm with a very short displacement of 2 to 3 mm. In the case of the PA2200 material samples shown in figure 4, graph *d*, it was shown that the SLS-made models exceeded, also by almost double the maximum force in comparison to the PLA material models, and the graphs did not show any particular localized jumps or significant decrease in the force acting on the models, or as in the case of the PLAW material graphs for samples 1 and 4 in the range of 2.25÷3 mm the collapse of the upper part of the model.

The PLAG and PLAW material specimens showed multiple arm kinks in the 1÷3 mm range as indicated by graphs *b* and *c* in figure 5. In contrast to the pre-vious samples with 5 mm and 6 mm side values, the samples manufactured from PLAB material showed that, for a given compressive force, the samples reached at 3 mm strain closer to the 5 mm side values and did not show a significant effect on the shoulders, i.e. kinking as in the case of the 6 mm side samples. A similar situation occurred, i.e. for the other samples manufactured from the PA2200 material by SLS tech-nology.

Referring to figure 6, one can notice a uniform distri-bution of force for samples manufactured by using SLS technology, as evidenced by table VI, which character-izes the correlation between the side and maximum force values. In contrast to SLS technology, for FDM

technology, individual models behave extremely chaotically despite the applied force, and models made of PLAG material show an unusual phenomenon of local collapse, shown in figure 4, where the appropriate places of model deflection and the overlapping of the arms are marked. In the case of the PLAB material, an almost uniform distribution of force can be observed regardless of the increase in the side value for $a = 6$ and 7 mm. In the case of the PLAW material, an uneven distribution of values can also be observed, but only for models with a side of 5 mm there are significant discrepancies between the force values for the test with a displacement of 3 mm.

Based on table V, the values are shown to be statistically significant at a significance level of $p = 0.05$ for 3 of the 4 materials in each of the aspects presented. For each of the materials, it was shown that for the three pairs of relationships, the values for the PA2200 material are the most strongly correlated. For each of the materials, it was shown that for Side-Load and Mass-Load relationships, there is a relationship that as the first characteristic increases, the values of the second characteristic decrease. In addition, by demonstrating the relevant characteristics, it can be concluded that for the PLAB material the previously mentioned characteristics were not statistically significant, which gives grounds to reject the test results shown previously for this material.

Conclusions

On the basis of the research results presented, formulate the following conclusions:
● As a result of the same STL model from which the hexagonal cell structures were manufactured, models with different mechanical properties were made, despite the PLA materials being similar. By contrasting the samples manufactured in FFF and SLS technology, it can be seen that the results of the hexagonal structures in each of the assumed configurations for SLS technology oscillate around similar values in contrast to the cell structures made in FFF technology, with no particular spikes and dips in the force acting on the model at deformations larger than 3 mm.
● By using different PLA materials to manufacture a fragment of a hexagonal cell structure, it should be noted that when comparing the results and plots with those of for the PA2200 material, the PLAB material samples showed progressively better mechanical properties with increasing side length.
● Samples manufactured from PA2200 material showed the most concentrated values for the 5 mm side, however, these samples, due to their size, scored a faster decrease in force at 5 mm strain compared to samples with 6 and 7 mm sides. Additionally, it was noted that as the side increased, the standard deviation of the maximum force also increased relative to the other models.
● The worst choice of material proved to be PLAG material for the assumed models. This is due to the fact that for each test the samples collapsed and were character-

ized by a rapid decrease in forces compared to models manufactured using the same technological parameters for the printing and compression test, despite a slight difference in mass for each group of test samples.
● Models of cell structures generated using the recursive formula showed that the size of the cell is not important to generate the appropriate size of cell structure.
● As a result of the tests, a suitable research direction was identified. This will concern the fractality of cell structures printed using incremental technologies and an attempt to juxtapose fractal cell structures with the presented concept of 2D repetitively generated cells. Future research will be concerned with demonstrating the correlation of whether cell structures or material influences the fractality of generated cells.
● Based on the test carried out on the correlation of the relationships, i.e. mass, load and side length, for the materials PA2200, PLAG, PLAW, PLAB, it should be stated that statistical significance was demonstrated for all assumed relationships for the materials PA2200, PLAG, PLAW. For each case, it was shown that for Side-Load and Mass-Load relationships, as the value of the first variable increases, the second variable decreases. However, for the PLAB material, it was shown that there is no statistical significance for the listed trait relationships for a variation level of $p = 0.05$, where the values are below 0.5139.

REFERENCES

[1] Oleksy M., Budzik G., Bolanowski M., Paszkiewicz A. "Industry 4.0. Part II. Conditions in the area of production technology and architecture of IT system in processing of polymer materials". *Polimery*. 64 (2019): 348–352, https://doi.org/10.14314/polimery.2019.5.5.

[2] Kozior T., Mamun A., Trabelsi M., Sabantina L. "Comparative Analysis of Polymer Composites Produced by FFF and PJM 3D Printing and Electrospinning Technologies for Possible Filter Applications". *Coatings*. 12 (2022): 48, https://doi.org/10.3390/coatings12010048.

[3] Cao D., Bouzolin D., Lu H., Griffith D.T. "Bending and shear improvements in 3D-printed core sandwich composites through modification of resin uptake in the skin/core interphase region". *Composites*. Part B: *Engineering*. 264 (2023): 110912, https://doi.org/10.1016/j.compositesb.2023.110912.

[4] Qi J., Chen Z., Jiang P., et al. "Recent Progress in Active Mechanical Metamaterials and Construction Principles". *Advanced Science*. 9 (2022): 2102662, https://doi.org/10.1002/advs.202102662.

[5] Vodilka A., Koroľ M., Kočiško M., Zajac J. "Adjusting Surface Models of Cellular Structures for Making Physical Models Using FDM Technology". *Polymers*. 15 (2023): 1198, https://doi.org/10.3390/polym15051198.

[6] Ghazlan A., Nguyen T., Ngo T., et al. "Performance of a 3D printed cellular structure inspired by bone". *Thin-Walled Structures*. 151 (2020): 106713, https://doi.org/10.1016/j.tws.2020.106713.

[7] Cao D. "Strengthening the interphase of thermoplastic sandwich composites by interleaving carbon nanotube yarns". *Materials Today Communications*. 36 (2023):106655, https://doi.org/10.1016/j.mtcomm.2023.106655.

[8] Bochnia J., Blasiak M., Kozior T. "A comparative study of the mechanical properties of fdm 3D prints made of PLA and carbon fiber-reinforced PLA for thin-walled applications". *Materials*. 14, 22 (2021), https://doi.org/10.3390/ma14227062.

[9] Cao D. "Enhanced buckling strength of the thin-walled continuous carbon fiber–reinforced thermoplastic composite through dual coaxial nozzles material extrusion process". *The International Journal of Advanced Manufacturing Technology*. 128 (2023): 1305–1315, https://doi.org/10.1007/s00170-023-12014-8.

[10] Kadhum A.H., Al-Zubaidi S., Abdulkareem S.S. "Effect of the Infill Patterns on the Mechanical and Surface Characteristics of 3D Printing of PLA, PLA+ and PETG Materials". *ChemEngineering*. 7 (2023): 46, https://doi.org/10.3390/chemengineering7030046.

[11] Kozior T., Kundera C. "Rheological properties of cellular structures manufactured by additive PJM technology". *Tehnicki Vjesnik*. 28, 1 (2021): 82–87, https://doi.org/10.17559/TV-20191007145545.

[12] Szot W. "Rheological Analysis of 3D Printed Elements of Acrylonitrile Butadiene and Styrene Material Using Multiparameter Ideal Body Models". *3D Printing and Additive Manufacturing*. (2023), https://doi.org/10.1089/3dp.2022.0298.

[13] Bochnia J., Blasiak S. "Stress relaxation and creep of a polymer-aluminum composite produced through selective laser sintering". *Polymers*. 12, 4 (2020), https://doi.org/10.3390/POLYM12040830.

[14] Zhang X., Yu X., Chen J., et al. "Influence Mechanism of the Trabecular and Chamfer Radii on the Three-point Bending Properties of Trabecular Beetle Elytron Plates". *Journal of Bionic Engineering*. 18 (2021): 409–418, https://doi.org/10.1007/s42235-021-0025-z.

[15] Gaur A., Chawla K., Kiran R., Patel S. "Effective thermo-electro-mechanical properties of Menger sponge-like fractal structures: a finite element study". *Physica Scripta*. 98 (2023): 095104, https://doi.org/10.1088/1402-4896/ace5f1.

[16] Płatek P., Rajkowski K., Cieplak K., et al. "Deformation Process of 3D Printed Structures Made from Flexible Material with Different Values of Relative Density". *Polymers*. 12 (2020): 2120, https://doi.org/10.3390/polym12092120.

[17] Mazurkiewicz M., Kluczyński J., Jasik K., et al. "Bending Strength of Polyamide-Based Composites Obtained during the Fused Filament Fabrication (FFF) Process". *Materials*. 15 (2022): 5079, https://doi.org/10.3390/ma15145079.

[18] Ullah A.S., D'Addona D.M., Seto Y., et al. "Utilizing Fractals for Modeling and 3D Printing of Porous Structures". *Fractal and Fractional*. 5 (2021): 40, https://doi.org/10.3390/fractalfract5020040.

[19] Haftendorn D. "Fraktale, Chaos, Ordnung". In: "*Mathematik sehen und verstehen. Spektrum*". Heidelberg: Akademischer Verlag, (2010): 79–116.

[20] "Technical Data Sheet PLA", (2018), https://www.google.pl/url?sa = t&rct = j&q = &esrc = s&source = web&cd = &cad = rja&uact = 8&ved = 2ahUKEwiKvPS0i4iAAxXgVaQEHbW4DM8QFnoECCYQAQ&url = https%3A%2F%2Fwww.matterhackers.com%2Fr%2F9EBLeA&usg = AOvVaw3A-QLWiVDQN6E0md5-VEix7&opi = 89978449 (dostęp: luty 2024).

[21] EOS. "Technical Data Sheet PA2200", (2023), https://www.materialdatacenter.com/mb/material/pdf/30963/30963/PA2200Performance1.0 (dostęp: luty 2024).

[22] "Makerbot". In: "*MakerBot Sketch – user manual*", (2022), https://cadxpert.pl/drukarki-3d/makerbot-sketch/ (dostęp: luty 2024).

[23] Stoia D., Linul E., Marsavina L. "Influence of Manufacturing Parameters on Mechanical Properties of Porous Materials by Selective Laser Sintering". *Materials*. 12 (2019): 871, https://doi.org/10.3390/ma12060871. ∎